High Speed Optical Interconnection using Embedded PDs on Electrical Boards

Sang-Yeon Cho, Jeff D. Hall, Ananthasayanam Chellappa,
Nan Marie Jokerst, and Martin Brooke
School of Electrical and Computer Engineering
NSF Electronic Packaging Research Center
Georgia Institute of Technology
E-mail: sycho@ece.gatech.edu

Abstract

As the data rate of electronic circuitry dramatically increases, interconnection speed becomes one of the critical bottlenecks in the overall performance of current data processing systems. A number of alternative approaches have been suggested to improve the current interconnection performance in terms of operational speed, power consumption, and area [1, 2, 3, 4]. As an alternative for current electrical interconnections, optical interconnections offer several attractive features. Advantages of optical interconnections include low power consumption, a significant reduction in interconnect footprint, and robust signal quality in high density interconnection systems because of immunity to electromagnetic interference.

There are a number of approaches toward the integration of optical signals into an electrical interconnection system. One approach utilizes waveguides and beam turning devices (e.g. mirrors, gratings) to address surface normal photodetectors (PDs) and vertical cavity surface emitting lasers (VCSELs) which can be bump bonded onto the module. A second approach also utilizes waveguides, however, the PDs and/or edge emitting lasers (EELs) are embedded in the waveguide/substrate sample, as shown in Figure 1, and evanescent field or direct coupling from the waveguide to the PD can be used to address the PD. This approach achieves alignment through assembly and successive masking layers and does not need optical beam turning devices. Thus, this optical interconnection integration mimics the transition in electronics from discrete packaged components to integrated circuits in the 1970s, through the integration of these embedded optical interconnections and active components.

A great deal of research to date has focused upon the implementation of polymer optical waveguides with standard electrical interconnection substrates, and there have been demonstrations of polymer waveguides addressing PDs fabricated in Si and GaAs substrates. This paper describes the heterogeneous integration of independently optimized polymer waveguides, embedded thin film InGaAs PDs operating at a wavelength of 1300 nm, and a standard Si substrate; thus using a different material for each of the three components in the embedded optical waveguide interconnection. Finally, an integrated circuit is attached to the electrical interconnection substrate and wire bonded to the embedded PD, as shown in Figure 1. This work represents steps toward chip to chip embedded optical interconnections integrated with electrical interface circuitry.

To create the embedded optical interconnection, thin film inverted metal-semiconductor-metal (I-MSM) PDs were fabricated and bonded to metal contacts on a SiO_2/Si substrate. Thin film I-MSM PDs were fabricated by mesa etching and a substrate removal process. The final thickness of the thin film PDs was 0.9 μm. The as-grown I-MSM material was InP/InGaAs (stop etch layer) / $Al_{0.48}In_{0.52}As$ graded to $In_{0.53}Ga_{0.47}As$ (600 Å)/ $In_{0.53}Ga_{0.47}As$ (0.74 μm thick absorbing layer)/ $In_{0.53}Ga_{0.47}As$ graded to $Al_{0.48}In_{0.52}As$ (600 Å)/ $Al_{0.48}In_{0.52}As$ (400 Å cap layer). Schottky contacts of 40 Å Pt/ 350 Å Ti/ 400 Å Pt/ 2500 Å Au were deposited, and interdigitated fingers 100 μm long with 2 μm finger width and 2 μm finger spacing were defined on a 100 μm x 150 μm detection area. After removing the growth substrate (InP) using selective chemical etching, each thin film device was transferred onto the metal contacts on a SiO_2/Si substrate. The waveguide fabrication process was then performed to embed the photodetector in the polymer waveguide. Benzocyclobutene (BCB 3022) was used as the waveguide core layer, and was spin coated onto the PD/SiO_2/Si. The BCB planar waveguide was patterned into a 100 μm wide channel waveguide using a thick photoresist mask and SF_6/O_2 dry etching.

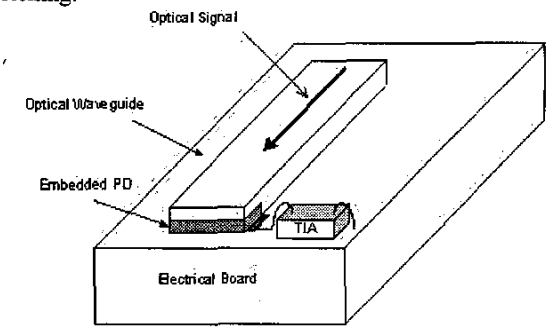

Figure 1. A schematic view of polymer optical interconnection using embedded PDs on electrical board.

Embedded thin film photodetectors in polymer waveguides for interconnections have been fabricated and tested. Typical results for these InGaAs embedded PDs (multiple samples have been fabricated) include a dark current of less than 10 nA after the polymer waveguide process and a surface normal responsivity of 0.38 A/W. At a wavelength of 1.3 μm, the coupled optical signal from the waveguide to the embedded photodetector was theoretically modeled at 56.4%, which was supported by an experimental estimate of 47.8%.

The measured FWHM of the electrical pulse from the MSM photodetector embedded in the waveguide was 16.73 ps for an input 500 femtosecond optical laser pulse. These PDs embedded in waveguides have also been connected to transimpedance amplifiers, and operated at speeds up to 100 Mbps.

Introduction

Chip to chip optical interconnections at the board and module become increasingly interesting with rising channel speed if compact, low loss, high data rate optical interconnections can be integrated into electrical interconnection systems. The potential for mask-based alignment of the optical interconnection waveguide, optoelectronic active devices, and interface circuits is attractive from a packaging alignment standpoint. This paper describes an integration process for creating optical interconnections which can be integrated in a post-processing format onto standard boards, modules, and even integrated circuits. These optical interconnections utilize active thin film (approximately 1-5 microns thick) optoelectronic components embedded in the waveguide/interconnection substrate. Since the optical coupling occurs using either direct or evanescent coupling into (laser) or out of (photodetector) the waveguide, the need for optical beam turning elements and their alignment is eliminated. This scheme essentially provides electrical inputs and outputs on the substrate from an optical interconnection. These embedded optical interconnections are reported herein using BCB polymer optical waveguides with embedded InGaAs-based thin film I-MSM photodetectors on a Si substrate.

A number of comparisons of electrical and optical interconnections have been published [5], and the topic of how to integrate chip to chip optical interconnections into an electrical interconnection system is currently under intensive study. Optical interconnect approaches include free space interconnects with diffractive optical elements [6], silicon optical bench interconnects [7], and guided wave interconnections, including integrated waveguides [8]. This paper focuses on embedded waveguide chip to chip optical interconnections which are integrated directly onto electrical interconnection boards and modules.

Integration Options For Embedded Optical Chip to Chip Interconnections

The embedded chip to chip optical interconnections described herein utilize optical signals which can originate and/or terminate in the waveguide directly on the board or module without optical beam turning. Figure 2 illustrates some of the options for embedding a detector in a waveguide, including embedding in the core (Figure 2a), and in the cladding (Figure 2b). Optical interconnections with integrated waveguides and OE devices in the substrate and epilayers [9, 10, 11] have been reported in compound semiconductors, such as InP-based materials, with reported high coupling efficiency and monolithic integration. However, the use of polymer waveguides and low cost epoxy and polymer substrates is interesting for chip to chip optical interconnections in electrical interconnection systems, and thus the emphasis in this paper on polymer waveguides for low cost optical interconnection which can be integrated with substrates such as high temperature FR-4. Polymer waveguides integrated onto Si [12] or GaAs [13, 14] electrical interconnection substrates which have photodetectors fabricated in the substrate have been reported. However, this approach excludes epoxy and polymer substrates since high performance photodetectors cannot be fabricated in these materials. The embedded waveguide approach reported herein uses thin film OE devices (with the OE device growth substrate removed) which can be bonded to any host substrate, including polymer and epoxy boards such as FR-4. The polymer waveguide material can then be deposited directly under or on top of the thin film active OE devices, which are thus embedded directly in the waveguide or cladding, as illustrated in Figures 2a and 2b, respectively. Circuits can be interconnected to the PDs using either bump or wire bonds, as illustrated in Figures 2c and 2d, respectively.

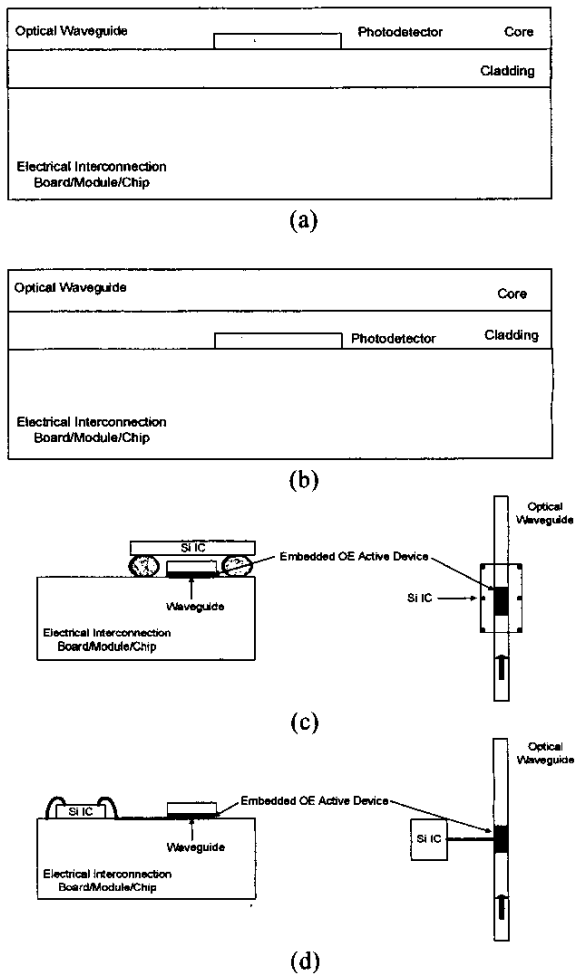

Figure 2. Integration options: (a) direct coupling; (b) evanescent coupling; (c) bump bonding of the circuit to the embedded PD; (d) wire bonding of the circuit to the embedded PD.

Fabrication

To embed a thin film InGaAs PD in a polymer waveguide, as illustrated in Figure 3a, the PD fabrication and waveguide fabrication must be co-optimized. A number of structures have been demonstrated. In this paper, impulse response and coupling data was taken on a photodetector embedded in a BCB waveguide with 1 μm of BCB core below the PD, and 5.3 μm of BCB core above it. This structure was integrated onto a Si/SiO_2 (3 μm thick) substrate. A second structure that was tested was a PD embedded in a waveguide integrated onto a Si/SiO_2 (3 μm thick) substrate, which had 2.7 μm of BCB (core waveguide layer) on the same size and structure PD. This sample had a Si CMOS foundry transimpedance amplifier (TIA) wire bonded to the PD. To begin both of the integrated samples, on the Si substrate (which is the electrical interconnection substrate), a 3 μm layer of SiO_2 was deposited onto the Si using plasma enhanced chemical vapor deposition (PECVD). For the first sample, this was followed by a spin coated 1 μm thick Benzocyclobutene (BCB) core layer followed by a cure at 240 ^{0}C for 1 hour. The 3 μm thick SiO_2 layer acts as a cladding and buffer layer for the BCB waveguide. Contact pads of Ti/Au (400 Å/ 5000 Å) were deposited and patterned on this substrate. Next, the thin film PDs were separately fabricated and bonded to the pads on the Si substrate. For the second sample, the PDs were bonded directly to the same contact pads which were deposited directly onto the SiO_2, and the 2.7 μm of BCB were spin coated on top of the PD and cured.

The thin film PDs were metal-semiconductor-metal (MSM) photodetectors which had the substrate removed, and the fingers on the bottom of the device. These are inverted MSMs (I-MSMs), which have a higher surface normal responsivity than conventional MSMs since the finger shadowing is eliminated [15]. When the I-MSMs and optical mode intensity distribution in the waveguide is co-optimized, these PDs can offer high speed, high responsivity operation with a large area and low capacitance. MSMs have larger area per unit capacitance than PiN devices at the same speed, which make them attractive candidates for high speed operation in interconnection systems. TIAs can only input limited capacitance from the PD, and, as speeds rise, PD areas decrease. Thus, to ensure adequate input signal to the TIA, large area (for a higher level of coupled signal), low capacitance PDs are essential.

The I-MSM photodetectors were independently fabricated and subsequently bonded to the metal contact pads on each substrate. The as-grown MSM material was InP/InGaAs (stop etch layer) / $Al_{0.48}In_{0.52}As$ cap layer (400 Å)/ $Al_{0.48}In_{0.52}As$ graded to $In_{0.53}Ga_{0.47}As$ (600 Å)/ $In_{0.53}Ga_{0.47}As$ (0.74 μm thick absorbing layer)/ $In_{0.53}Ga_{0.47}As$ graded to $Al_{0.48}In_{0.52}As$ (600 Å)/ $Al_{0.48}In_{0.52}As$ cap layer (400 Å). Schottky contacts of 40 Å Pt/ 350 Å Ti/ 400 Å Pt/ 2500 Å Au were deposited, and interdigitated fingers 100 μm long with 2 μm finger width and 2 μm finger spacing were patterned on a 100 μm x 150 μm absorbing area. The 400 Å thick Pt layer acts as a diffusion barrier to the Au during the polymer waveguide thermal curing process [16]. Using the Pt diffusion barrier on the MSM means that the Schottky barriers are not degraded by the waveguide thermal process, and thus, the dark current is not degraded by the integration process. Then, each MSM device was mesa etched down to the InP substrate layer using a citric:H_2O_2 (10:1) selective etch. The MSM mesas were patterned with Apiezon W wax and immersed in HCl to selectively remove the InP substrate, stopping on the InGaAs layer. The thin film MSM mesa devices in the Apiezon W wax were then bonded to a mylar transfer medium. The Apiezon W was dissolved with trichloroethylene, leaving the thin film MSM devices bonded to the mylar transfer diaphram. The thickness of these MSM devices was 0.9 μm.

Next, the thin film MSMs were transferred onto the each substrate (metal pads on either a BCB or SiO_2 surface), and the waveguide integration to embed the I-MSMs was then completed by spin coating the waveguide layer onto the PD. The MSMs were transferred using the mylar transfer diaphragm [17], and were bonded to the metal pads on the $BCB/SiO_2/Si$ substrate, thus inverting the device (creating the I-MSM). This metal (I-MSM pad) to metal ($BCB/SiO_2/Si$ substrate pad) bond is an electrically conducting, mechanically stable bond created using a low temperature anneal of 10 minutes at 150 ^{0}C, which was used after the device was bonded to the contact pads. The waveguide fabrication process was then continued to embed the photodetector in the polymer waveguide. In both samples, BCB was spin coated onto the sample and cured at 240 ^{0}C for 1 hour. All BCB thermal cures were carried out in a nitrogen ambient to avoid oxidation of the BCB, since oxidization can slightly increase the refractive index of the film [18].

To complete the waveguide integration process, the first sample's BCB was polished, and both samples' waveguides were etched into channels. For the first sample, to minimize the scattering loss due to the surface roughness of the core layer, the BCB top layer was chemi-mechanically polished (CMP) using Rodel 3116B, deionized water, and a slurry abrasive of 0.05 μm Al_2O_3. The final thickness and surface roughness of the core layer for the first sample were 6.3 μm, and 600 Å respectively, as measured by a profilometer. Both BCB planar waveguides were then patterned into 100 μm wide channel waveguides using a photoresist mask and SF_6/O_2 reactive ion etching. The width of the fabricated waveguide matched the detection area (100 μm × 150 μm) of the embedded PD to maximize the coupling efficiency from the waveguide to the embedded PD. The 100 μm wide BCB waveguide channel was positioned over the center of inverted MSM photodetector, so the guided optical signal was incident on the high electrical field interdigitated finger region of the embedded I-MSM photodetector. Thus, carriers photogenerated by direct coupling from the waveguide into the photodetector are effectively swept into the interdigitated finger contacts. Figure 3 is a photomicrograph of the first sample, which is an I-MSM PD embedded in a BCB polymer waveguide (with an under and over layer) on a SiO_2/Si substrate. Figure 4 is a photomicrograph of the second sample, which is an I-MSM PD embedded in a BCB polymer waveguide on a SiO_2/Si substrate.

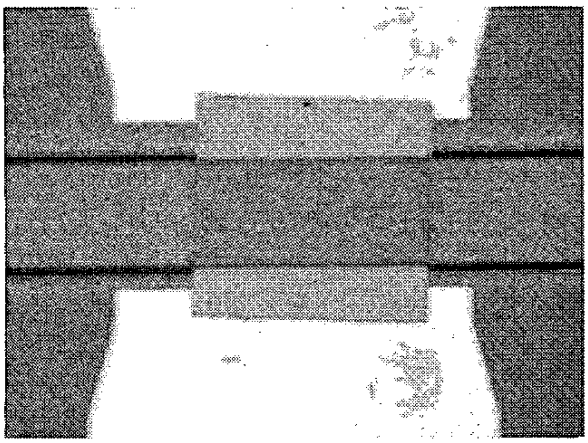

Figure 3. Sample 1: I-MSM embedded in a polymer channel waveguide.

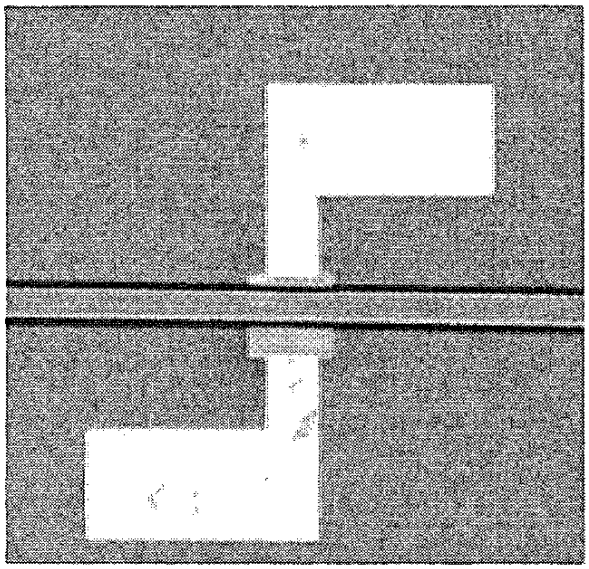

Figure 4. Sample 2: I-MSM embedded in a polymer channel waveguide.

For the second sample, the TIA was bonded to the SiO_2/Si substrate with epoxy, as shown in Figure 5. The TIA was then wirebonded to the embedded PD as well as the bias and signal lines on the SiO_2/Si substrate. The entire SiO_2/Si substrate was then bonded to the FR4 testboard with epoxy as shown in Figure 5. The signal and bias lines were then wirebonded to the testboard.

Device characterization

The I-MSM dark current and photoresponse were measured before and after waveguide fabrication for Sample 1. The photoresponse before integration was measured in a surface normal configuration, in the embedded waveguide configuration after the waveguide was integrated onto the PD.

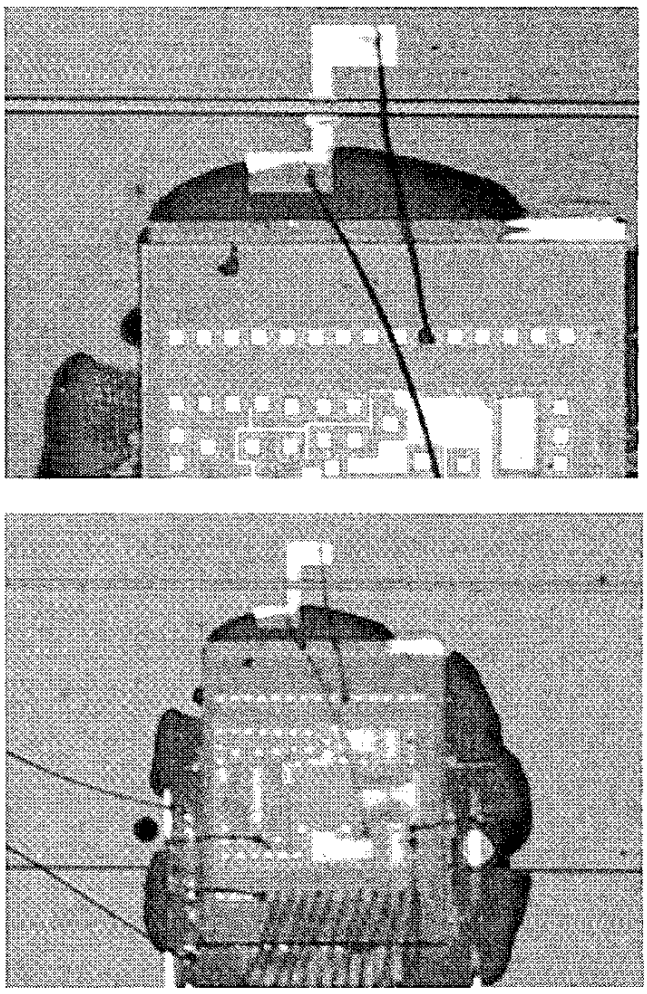

Figure 5. Sample 2: Embedded I-MSM PD in the BCB polymer waveguide on the SiO_2/Si substrate.

A fiber pigtailed laser diode connected to a 62.5 μm multimode fiber was used for the optical input for the surface normal responsivity. The optical power output from the fiber was 1.54 mW. The I-MSM surface normal responsivity without an AR coating had a measured responsivity of 0.38 A/W at 5 V. After the waveguide integration, to test the waveguide coupling on Sample 1, the Si substrate was cleaved to produce an endface on the polymer waveguide, and a single mode optical fiber (core diameter = 9 μm, Numerical Aperture (NA) = 0.13) was endface coupled to the polymer waveguide. Figure 6 shows the measured dark current before and after the polymer optical waveguide process, and the photocurrent due to the coupling from the waveguide to the I-MSM PD embedded in the waveguide. The dark current, which is 5.2 nA at 5 V before waveguide integration, and 4.8 nA at 5 V after waveguide integration, has improved slightly after the waveguide process, which may be due to annealing of the I-MSM Schottky contacts. The photocurrent at 5 V was 42.02 μA. Thus, the optical signal in the waveguide has been successfully coupled into the embedded photodetector.

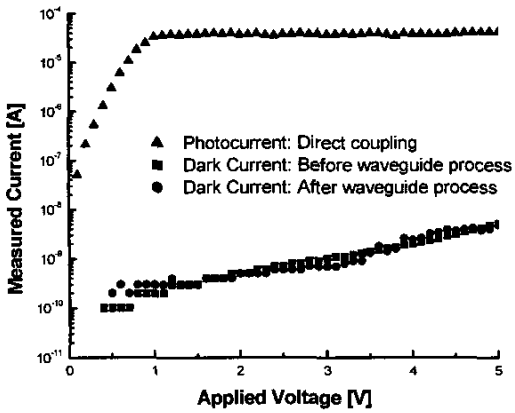

Figure 6. Dark current before and after waveguide integration process, and photocurrent due to direct coupling.

The propagation loss of the integrated channel polymer waveguide was measured in Sample 1 using an optical fiber scanning method. The probing large core multimode fiber (core diameter = 600 μm, NA = 0.37) measures the scattered optical signal from the channel waveguide. This optical fiber was set at the same height (within a cm) from the sample while 300 scanning points (using a motorized micro-positioner), which were measured perpendicular to the waveguide in 10 μm increments. These 300 points constitute one scan line. There were 300 scan lines measured, each separated by 10 μm. The propagation loss per unit distance was calculated by the slope of the linear least square regression line of the average collected optical power from the waveguide before the detector. Using this method, the estimated propagation loss of the BCB polymer channel waveguide was 0.36 dB/cm at a wavelength of 1.3 μm. This estimate includes intrinsic material, structural, and other propagation loss sources for the polymer optical waveguide, which is consistent with other reported results for BCB waveguides [19, 20].

The electrical pulse response to a short optical pulse was measured for the embedded thin film I-MSM photodetector fabricated in Sample 1. A 500 femtosecond Full-Width-Half-Maximum (FWHM) fiber laser was used as the light source in this speed measurement, and was endface coupled through a lensed single mode optical fiber (minimum spot size = 5 μm) into the Sample 1 BCB polymer waveguide. The electrical response from the embedded thin film MSM photodetector was probed through a 40 GHz GS (Ground Signal) microwave probe, and the pulse was measured with a Tektronix 50 GHz sampling oscilloscope. The pulse response from the embedded I-MSM photodetector in Sample 1 is shown in Figure 7. The measured FWHM output of the I-MSM electrical output pulse was 16.73 ps at 3.5 V.

The measured pulse response of the embedded I-MSM photodetector is very fast, particularly considering the large area of this photodetector (100 μm X 150 μm).

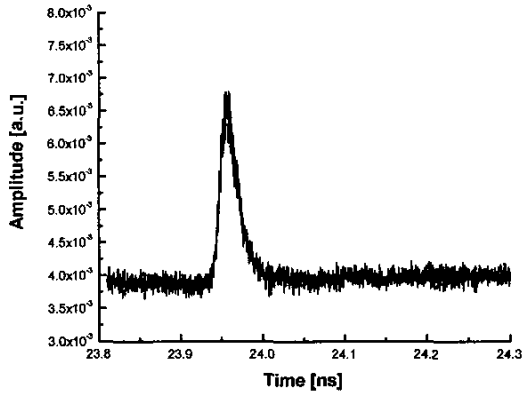

Figure 7. Impulse response from Sample 1.

By comparison, other published MSM photodetectors which run at similar speeds are on the order of 30 μm in diameter [21, 22]. One factor which may explain this improvement in speed for the embedded I-MSM is the well confined electric field lines in the I-MSM, which is surrounded by low dielectric constant BCB. Thus, the electric field confinement in the thin film embedded I-MSM is better than in conventional MSMs on the growth compound semiconductor substrate. These large area I-MSMs are critical for high speed optical interconnect, where detector size may limit the coupling efficiency.

Coupling Efficiency Characterization

Several theoretical analysis approaches have been suggested for photodetectors integrated with optical waveguides. One of the most commonly used analysis methods for integrated waveguide/photodetector structures is the Beam Propagation Method (BPM) [23, 24]. However, there are some restrictions associated with the conventional BPM method when modeling high index contrast in the structure and reflected traveling beams. In the models presented herein, the high index contrast problem between the polymer optical waveguides and the embedded photodetectors and the possible reflections at the interfaces between the input waveguide regions and the embedded regions were addressed with wide angle and bi-directional BPM.

The coupling from the waveguide to the PD can be modeled and estimated, but it is difficult to precisely measure the coupling for an embedded PD due to the difficulty in estimating the fiber to waveguide endface coupling. In this paper, the waveguide to I-MSM coupling efficiency is theoretically calculated, and also estimated from measurement results. The theoretical models were generated using RSoft, a BPM modeling software package. The estimated coupling efficiency from Sample 1, the 6.3 μm thick multimode waveguide into the 150 μm long embedded I-MSM PD, was 56.4% using scalar wave analysis.

The coupling efficiency from the waveguide to the embedded I-MSM PD was also estimated through measurement for Sample 1. The measured output from the single mode optical fiber was 1.54 mW. Using scalar BPM,

an estimated 16.7% of this optical signal was coupled into the waveguide. The optical signal travels 1.19 cm from the fiber input to the detector, which causes a loss of 0.43 dB (using the measured -0.36 dB/cm measured propagation loss). So the estimated optical power incident on the embedded detector in the waveguide is 0.23 mW. To calculate the PD absorbed optical power, divide the photocurrent (42.02 μA) from the embedded photodetector (when it is excited through coupling in the waveguide) by the PD surface normal responsivity (0.38 A/W), and thus, 0.11 mW of optical power was absorbed by the photodetector. The estimated coupling efficiency is the absorbed power divided by the incident power, which is 47.8%. This agrees fairly well with the theoretical coupling efficiency (56.4%). Although this estimate of the measured coupling efficiency is very rough, it does indicate that enough coupling can be achieved to create a viable interconnect. One of the attractive aspects of this integration technology is that the coupling can be intentionally varied through structural design so that the majority of the optical signal can be detected, or a fraction of the signal can be detected, thus reserving signal for subsequent PDs which can be located further down the optical path on the same waveguide.

Test of Embedded Optical Interconnection with a Si CMOS Transimpedance Amplifier

The second sample, in which a Si CMOS TIA was wire bonded to the PD embedded in a polymer waveguide, as shown in Figure 5, was tested using a distributed feedback (DFB) single mode fiber coupled laser operating at a wavelength of 1.55 μm. An external modulator was used to modulate the signal, and the output of the modulator was 2 mW. The modulator single mode fiber output was endface coupled into the waveguide. The output of the PD embedded in the waveguide was 71.02 μA when the fiber was endface coupled. Figure 8 is an eye diagram at 25 Mbps from Sample 2, and Figure 9 is an eye diagram at 100 Mbps from Sample 2. Both used PSRB 2^7. Better decoupling will enable this system to operate at much higher speeds in the future.

Conclusions

Significant opportunities exist for optical interconnections at the board and module level if compact, low loss, high data rate optical interconnections can be integrated into these substrates. To realize such an integrated optoelectronic microsystem, mask-based alignment of the optical interconnection waveguide, optoelectronic active devices, and interface circuits is attractive from a packaging alignment standpoint. This paper describes an integration process for creating optical interconnections which can be integrated in a post-processing format onto standard boards (including polymer and epoxy) and modules, and eventually, even integrated circuits. These optical interconnections utilize active thin film optoelectronic components embedded in the waveguide/interconnection substrate, thus providing an electrical output to the user from an optical interconnection.

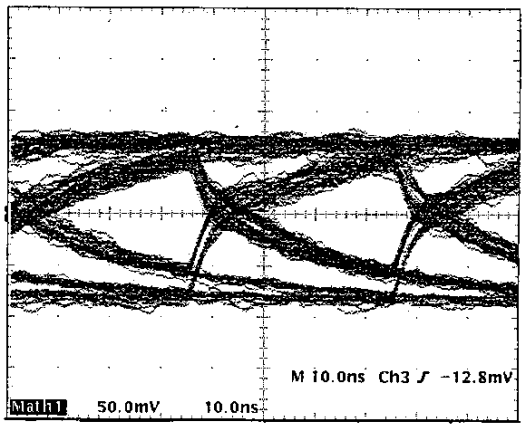

Figure 8. Eye diagram for Sample 2 at 25 Mbps.

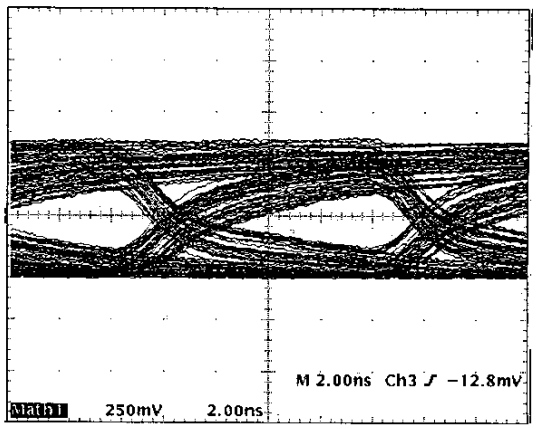

Figure 9. Eye diagram for Sample 2 at 100 Mbps.

These embedded optical interconnections have been demonstrated and reported herein using BCB polymer optical waveguides with embedded InGaAs-based thin film I-MSM photodetectors on Si substrates. Two samples have been fabricated and tested. In Sample 1, these interconnections demonstrated over 47% coupling efficiency. The measured FWHM of the electrical pulse from the embedded MSM photodetector was 16.73 picosecond for a 500 femtosecond optical input laser pulse. In Sample 2, the output of a thin film PD embedded in a polymer waveguide on a Si substrate was wire bonded to a TIA, and the system produced an eye diagram at 25 Mbps and 100 Mbps. The integration process reported herein for these embedded optical interconnections is consistent with integration onto electrical interconnection microsystems. Thus, there is promise for the incorporation of optical interconnections with standard electrical signals at the board, module, and integrated circuit level.

Acknowledgments

The authors would like to thank the National Science Foundation Electronic Packaging Research Center and the State of Georgia Yamacraw Program for their support of this work, and the staff of the Georgia Tech Microelectronics Research Center cleanroom for their support.

References

1. Mark Horowitz, Chih-Kong Ken Yang, Stefanos Sidiropoulos, " High-Speed Electrical Singaling: Overview and Limitations," *IEEE Micro*, 1998, pp. 12-24.
2. William J. Dally, John Poulton "Transmitter Equalization For 4-Gbps Signaling," *IEEE Micro*, 1997, pp. 48-56.
3. Changsik Yoo, "High-speed DRAM interface," *IEEE Poten.*, vol. 20, 2002, pp. 33-34.
4. Woonghwan Ryu, Junwoo Lee, Hyungsoo Kim, Seungyoung Ahn, Namhoon Kim, Baekkyu Choi, Donggun Kam, and Joungho Kim, "RF interconnect for Multi-Gbit/s Board-Level Clock Distribution," *IEEE Trans. on Adv. Pack.*, vol. 23, 2000, pp. 398-407.
5. David A. B. Miller, "Rationale and Challenges for Optical Interconnects to Electronic Chips," *Proc. of the IEEE*, vol. 88, 2000, pp. 728-749.
6. S. J. Walker and J. Jahns, "Optical clock distribution using integrated free-space optics," *Opt. Comm.*, vol. 90, 1992, pp. 359-371.
7. Rassaian, M.; Beranek, M.W., "Quantitative characterization of 96.5Sn3.5Ag and 80Au20Sn optical fiber solder bond joints on silicon micro-optical bench substrates," *IEEE Trans. on Adv. Pack.*, vol. 22, 1999, pp. 86-93.
8. B. Bihari, J. Gan, L, Wu, Y. Liu, S. Tang, and R. T. Chen, "Optical clock distribution in supercomputers using polyimide-based waveguides," *Proc., Opto. Intercon. VI.*, San Jose, CA, Jan. 1999, pp. 123-133.
9. St. Kollakowski, A. Strittmatter, E. Dröge, E. H. Böttcher, and Bimberg, "65 GHz InGaAs/InAlGaAs/InP waveguide-integrated photodetectors for the 1.3-1.55 μm wavelength regime," *Appl. Phys. Lett.*, vol. 74, 1999, pp. 612-614.
10. E. H. Böttcher, H. Pfitzenmaier, E. Dröge, St Kollakkowski, A. Stittmatter, and D. Bimberg, R. Steingrüber "Distributed waveguide-integrated InGaAs MSM Photodetectors for high-efficiency and ultra-wideband operation," *IEEE 11th Intern. Conf. on Indium Phosphide and Related Mat.*, 1999. pp. 79-82.
11. St. Kollakowski, E. Dröge, E. H. Böttcher, A. Strittmatter, O. Reimann, and D. Bimberg, "Waveguide-Integrated InP/InGaAs/InAlGaAs MSM Photodetector for Operation at 1.3 and 1.55 μm," *IEEE 10th Intern. Conf. On Indium Phosphide and Related Mat.*, 1998, pp. 266-268.
12. C. H. Buchal, A. Roelofs, M. Siegert, and M. Löken, "Polymeric strip waveguides and their connection to very thin ultrafast metal-semiconductor-metal detectors," *Mat. Res. Soc. Symp. Proc.* vol. 597, 2000, pp. 97-102.
13. François Gouin, Lucie Robitaille, Claire L. Callender, Julian Noad, Carlos Almeida, " A 4x4 optoelectronic switch matrix integrating an MSM array with polyimide optical waveguides," *SPIE*, vol. 3290, 1997, pp. 287-295.
14. C. L. Callender, L. Robitaille, J. P. Noad, F. Gouin, and C. Almeida, "Optimization of metal-semiconductor-metal (MSM) photodetector arrays integrated with polyimide waveguides," *SPIE*, vol. 2918, 1997, pp. 211-221.
15. Olivier Vendier, Nan Marie Jokerst, and Richard P. Leavitt, "Thin-Film Inverted MSM Photodetectors, " *IEEE Photon. Tech. Lett.*, vol. 8, 1996, pp. 266-268.
16. D. G. Ivey, P. Jian, Robert Bruce, Gordon Knight, "Microstructural analysis of Au/Pt/Ti contacts to p-type InGaAs," *Journ. of Mat. Sci.: Mat. in Electron.*, vol. 6, 1995, pp. 219-227.
17. Nan Marie Jokerst, Martin A. Brooke, Olivier Vendier, Scott Wilkinson, Suzanne Fike, Myunghee Lee, Elizabeth Twyford, Jeffrey Cross, Brent Buchanan, and Scott Wills, "Thin-Film Multimaterial Optoelectronic Integrated Circuits," *IEEE Trans. On Comp. , Pack., And Man. Tech., Part B*, vol. 1, 1996, pp. 97-106.
18. R. Kirchoff, C. Carriere. K. Bruza, N. Rondan, and R. Sammler, "Benzocyclobutenes: A new class of high performance polymer." *Journ. Macro. Sci.-Chem.*, vol. 28, 1991, pp. 1079-1113.
19. S. Wolff, A. R. Giehl, M. Renno, H. Fouckhardt, "Metallic waveguide mirrors in polymer film waveguides," *Appl. Phys. B*, vol. 73, 2001, pp. 623-627.
20. G. Fischbeck, R. Moosburger, M. Topper and K. Peterman, "Design concept for singlemode polymer waveguides," *Electron. Lett.*, vol. 32, 1996, pp. 212-213.
21. Y. G. Zhang, A. Z. Li, J. X. Chen, "Improved performance of InAlAs-InGaAs-InP MSM photodetectors with graded superlattice structure grown by gas source MBE," *IEEE Photon. Tech. Lett.*, vol. 8, 1996, pp. 830-832.
22. St. Kollakowski, E. H. Bottcher, A. Strittmatter, D. Bimberg, "High-speed InGaAs/InAlGaAs/InP waveguide-integrated MSM photodetectors for 1.3-1.55 mu m wavelength range," *Electron. Lett.*, vol. 34, 1998, pp. 587-589.
23. R. Scarmozzino, A. Gopinath, R. Pregla, and S. Helfert, "Numerical Techniques for Modeling Guided-Wave Photonic Devices," *IEEE Journ. of Select. Topics in Quan. Electron.*, vol. 6, 2000, pp. 150-162.
24. G. R. Hadley, "Wide-angle beam propagation using Pade approximant operators," *Opt. Lett.*, vol. 25, 1992, pp1426-1428.